Desalination and Water Treatment
www.deswater.com
doi: 10.5004/dwt.2020.26423

207 (2020) 185–196
December

Improving the photocatalytic activity of silver orthophosphate by thermal annealing for photocatalytic degradation of β-naphthol

Weiwu Hu[a,b,*], Yiyao Sun[a], Nan Chen[a,*], Chuanping Feng[a], Yang Deng[a], Hongyan Chen[c], Jibo Qin[a], Miao Li[d], Yu Gao[e]

[a]*School of Water Resources and Environment, MOE Key Laboratory of Groundwater Circulation and Environmental Evolution, China University of Geosciences, Beijing 100083, China, Tel. +86 10 82321904; Fax: +86 10 82321081; emails: 2007012116@cugb.edu.cn (W.W. Hu), chennan@cugb.edu.cn (N. Chen)*
[b]*The Journal Center, China University of Geosciences, Beijing 100083, China*
[c]*College of Science, Beijing Forestry University, Beijing 100083, China*
[d]*School of Environment, Tsinghua University, Beijing 100084, China*
[e]*College of Chemical and Environmental Engineering, Shandong University of Science and Technology, Qingdao 266590, China*

Received 7 January 2020; Accepted 3 August 2020

ABSTRACT

β-naphthol, a highly toxic compound, can be absorbed through the skin and exposure to it increases the incidence of dermatitis, conjunctivitis, and rhinitis. In this study, silver orthophosphate (Ag_3PO_4) photocatalyst was successfully prepared via a simple thermal annealing route to remove β-naphthol from water under simulated visible light. The characteristics of prepared photocatalyst were measured by scanning electron microscopy (SEM), X-ray photoelectron spectrometry (XPS), X-ray diffraction (XRD), UV-vis diffuse spectra (UV-vis DRS), and photoluminescence (PL). Moreover, the photocatalytic activity was studied using different parameters such as catalyst concentration, substrate concentration, reaction pH, humic acid concentration, and in the presence of various common anions. All parameters except solution pH were statistically significant. It can be observed that 98.5% of β-naphthol can be degraded. The active species trapping experiments indicated that both h^+ and $^{\bullet}O^{2-}$ played prominent roles in the photodegradation of β-naphthol. It also showed that the catalyst annealed at 400°C exhibited the best stability and reproducibility. In addition, this study identified the intermediate products produced during the reaction process to support the photocatalysis mechanism.

Keywords: Silver orthophosphate; Thermal annealing; β-naphthol degeneration; Visible light; Stability and regeneration

1. Introduction

Polycyclic aromatic hydrocarbons (PAHs) with two or more fused aromatic rings arranged linearly, angularly, and clustered, widely exist in the atmosphere, water, soil, and organism [1]. PAHs have been classified as priority pollutants by the United States Environmental Protection Agency (USEPA) due to their potential damage to human health and ecosystem [2]. β-naphthol is one of the most toxic compounds in typical industrial PAHs and their derivatives [3]. β-naphthol is mainly released from dye stuffs manufactory, pharmaceutical production, and some biogeochemical processes [4]. Every year a large amount of β-naphthol enters the aquatic ecosystems through industrial wastes. People are more likely to be infected by dermatitis, conjunctivitis, and rhinitis if they are exposed to β-naphthol since it can be absorbed by the skin. Moreover, β-naphthol combines with glucuronic acid and sulfate rapidly in the

* Corresponding authors.

excreta of the liver and kidney, which has adverse effects on the liver, kidney, and even the nervous system [5]. Therefore, effective removal of β-naphthol from wastewater before its discharge into the environment has gained considerable attention.

To date, various methods to eliminate β-naphthol from the contaminated water have been studied, including volatilization, electrochemical, and biological techniques [6–8]. However, these technologies have some limitations and shortcomings, such as incomplete mineralization, toxic by-products, or ineffective degradation. [6]. Because of its high mineralization efficiency and the ideal final product is the production of carbon dioxide, water and inorganic mineral ions, photocatalytic oxidation is a "green" technology for treating organic pollutants by simulated visible light [9,10]. Recently, several researchers have studied the photocatalytic degradation of β-naphthol by TiO_2, but it only can absorb radiation in the ultraviolet region due to its wide band gap of E_g = 3.2 eV, thus about 5.0% of sunlight can be exploited. It greatly limits the use of sunlight [11]. Therefore, it is urgent to find semiconductor materials that exhibit high photocatalytic activity under visible light.

Most recently, Ag_3PO_4 has attracted enormous attention due to its extremely high photooxidative capability for O_2 evolution from water and organic pollutants photodegradation under visible light irradiation [12]. More specifically, this novel photocatalyst exhibits an extremely high quantum yield of about 90.0% at wavelengths less than 480 nm [13], which means a very low electron–hole recombination rate. However, it is well-known that Ag_3PO_4 is slightly soluble in aqueous solution, and Ag^+ can be easily reduced into metal Ag by exciting electrons without any sacrificial photoexcitation [14]. This phenomenon showed that not only the structure of Ag_3PO_4 was destroyed, but also the light absorption efficiency of Ag_3PO_4 was reduced, thus its photocatalytic activity and stability were affected. In recent years, researchers have developed various strategies to address this issue, including morphology-control [15,16], plasmonassist [17,18], and hetero-coupling technologies [19–22]. In addition, hydrolysis method [23], solvothermal method [24], template method [25], and *in situ* chemical conversion [26] were also used for the preparation of catalytic materials. However, organic solvents and capping agents are usually needed to control the size and shape of the Ag_3PO_4 catalysts, and the catalytic efficiency of as-prepared Ag_3PO_4 products is also limited because of the inherent low porosity of these structures [27].

High temperature calcination can induce changes in physicochemical properties. It is a simple and effective approach to modify the photocatalytic activity of a semiconductor [28,29]. Yu et al. [30] reported that with the increase of calcination temperature, the photocatalytic activity of anatase TiO_2 increased gradually, and the increased photocatalytic efficiency was attributed to the increase of crystallization degree. Xu et al. [31] found that the g-C_3N_4 crystallized by high temperature calcination showed an extended visible light absorption and enhanced charge separation and transfer efficiency due to the formation of nitrogen defects. Xing et al. [32] also confirmed that high temperature calcination could promote the release of oxygen vacancies, which played an important role in improving the photocatalytic activity of TiO_2. Therefore, high temperature calcination is a potential method to produce synergistic effects to enhance photocatalytic activity, including Ag_3PO_4.

In this study, a novel Ag_3PO_4 photocatalyst was successfully prepared by a simple thermal annealing route. The morphology, structural characterization, chemical composition, spectroscopic, and separation rate of photogenerated carriers of Ag_3PO_4 before and after thermal annealing were studied by scanning electron microscopy (SEM), X-ray diffraction (XRD), X-ray photoelectron spectroscopy (XPS), UV-vis diffuse reflection spectrum (DRS), photoluminescence (PL), and zeta potential methods. The effects of photocatalyst dosage, initial substrate concentration, pH value, humic acid concentration, and metal ions on the photocatalytic degradation of β-naphthol were investigated. The mechanism of photocatalytic degradation was studied by active species capture experiment. At the same time, some intermediates produced in the reaction were analyzed.

2. Experimental

2.1. Preparation of samples

The pristine Ag_3PO_4 samples were prepared by an ion exchange method, which was described in pre literatures [33]. In a typical synthesis, the aqueous ammonia solution was slowly added to 100 mL $AgNO_3$ (0.2 mol/L) water solution under a constant magnetic stirring, affording a silver ammonia solution, until the brown precipitate was completely dissolved. Then, subsequently added 75 mL NaH_2PO_4 (0.2 mol/L) solution dropwise to the above solution and stirred for 120 min. The precipitates were collected by centrifugation, washed five times with ethyl alcohol and distilled water, afterwards dried at 60°C for 6 h. Then, the as-obtained Ag_3PO_4 samples were calcined in a muffle furnace at 400°C for 4 h, which were denoted as Ag_3PO_4-400.

The preparation methods of other catalyst (Ag_3PO_4/g-C_3N_4, Ag_3PO_4/WO_3, and Ag_3PO_4/ZnO) were referred to the reported articles [34–36].

2.2. Characterization

SEM (JSM-7001F, Shimadzu, Japan) was used to examine the morphology and structure of the as-prepared samples. The phase structures of the powders were evaluated by XRD (D8 Focus, Bruker, Germany). The chemical composition and state of the surface were studied by XPS (ESCALAB 250Xi, Thermo Fisher, USA). The UV-vis DRS was recorded in the wavelength range of 200–800 nm using the UV-vis near infrared spectrophotometer (Cary 5000, Varian, USA). PL spectra were recorded on a luminescence spectrometer (RF-5310PC, Shimadzu, Japan). A continuous wave 325 nm helium–cadmium laser was used as the excitation source at room temperature. The zeta potential was measured at various pH values with a micro electrophoresis instrument (JS94H, Shanghai, China).

2.3. Photocatalytic degradation experiment

In the photocatalytic system, 100 mL of aqueous solution containing the desired concentrations of β-naphthol was

loaded in a beaker at ambient temperature under continuous stirring. The amount of catalyst was 0.05, 0.10, 0.20, and 0.30 g, respectively, the initial concentration of β-naphthol was 10, 20, 30, and 50 mg/L respectively, and the initial pH value of the solution was 3.0, 5.0, 7.0, 9.0, and 12.0, respectively. Use a 0.1 M HNO_3 or 0.1 M NaOH solution to achieve the required pH. Different anions dosing with Cl^-, HPO_4^{2-}, SO_4^{2-}, and NO_3^-, different humic acid dosing concentrations with 0.5, 1.0, 5, and 10 mg/L. The photocatalytic activity of the prepared photocatalyst was investigated by using a 300 W xenon lamp to degrade β-naphthol solution under visible light (CEL-HXF300, China), and the irradiance used in the experiment was 40 mW/cm^2. The distance between the lamp and the surface of the reaction solution was 10 cm. Then, for establishing the adsorption–desorption equilibrium of the photocatalyst, the solution was stirred with a magnetic bar during 10 min in the darkness. Afterwards, the lamp was turned on and the reaction mixture was exposed to simulated solar irradiation. Sampling interval was 2 min, and analyze it with Agilent 1260 infinite high performance liquid chromatography (HPLC) system (1260 infinite, America) after filtered with 0.22 μm nylon membrane filter. Total organic carbon (TOC) analysis of the liquid samples was performed on Analytik Jena multi N/C 2100S, which was produced by Germany. The intermediate products were determined using a GC-MS system (Agilent 7890 A GC with 5975C Series mass spectrometry). Triplicate each test and report the average result.

3. Results and discussion

3.1. Characterization of as-prepared samples

The phase structure and the crystallinity of the pristine Ag_3PO_4 and Ag_3PO_4-400 were investigated by XRD. As shown in Fig. S1a, two samples displayed characteristic diffraction peaks (2θ) at 21.1°, 29.9°, 33.5°, 36.8°, 42.7°, 48.0°, 52.9°, 55.2°, 57.5°, 61.8°, 66.0°, 70.1°, 72.1°, and 74.0°. All diffraction peaks were in good accordance with the standard data (JCPDS No. 06-0505), which means that a pure Ag_3PO_4 phase with a body-centered cubic structure was obtained. It was notable that upon annealing in air, the peak intensity became sharper and stronger, suggesting that the crystallinity of Ag_3PO_4 became much better. Moreover, it was found from a partial enlargement in XRD diagram (Fig. S1b) that all the peaks of the calcined Ag_3PO_4-400 samples was significantly shifted to a higher angle than the pristine Ag_3PO_4, implying the contraction of Ag_3PO_4 lattice after annealing. Maybe the separation of the interior Ag atoms from the Ag_3PO_4 supercell lead to such contraction of Ag_3PO_4 lattices, leaving an isolated Ag vacancies within the heavily distorted AgO_4 tetrahedron [37].

Fig. S2a demonstrated the UV-vis DRS of pristine Ag_3PO_4 and Ag_3PO_4-400. It can be observed that both of the two Ag_3PO_4 samples showed similar absorption plot. In the visible region, the pristine Ag_3PO_4 had a broader absorption than the Ag_3PO_4-400, and the absorption edge is about 530 nm. It can be seen from Fig. S2b, the indirect energy gap of the original Ag_3PO_4 is estimated to be 1.67 ev. The energy gap of Ag_3PO_4-400 sample increases from 1.67 to 1.75 ev after heat treatment. A slight blue shift of Ag_3PO_4 band edge occurred with thermal annealing, which can be attributed to the difference in particle size associated with thermal treatment. In addition, there is no other absorption in the visible region, indicating that no impurities are produced during the calcination process.

The morphology of the pristine Ag_3PO_4 and Ag_3PO_4-400 catalysts were investigated using SEM analysis (Fig. 1). Figs. 1a and b show the SEM images of the original Ag_3PO_4 show that the original Ag_3PO_4 is composed of spherical particles with an average particle size of about 200 nm, and the particles are basically monodisperse. Figs. 1c and d show the SEM images of the Ag_3PO_4-400, and the Ag_3PO_4 particles became larger with the average size of 438 nm after being calcined at 400°C. Heat treatment greatly promotes the growth of these particles, and large particles are connected end-to-end, thus self-assembly into chain structure. The solution of Ag^+ in Ag_3PO_4-400 was inhibited by the close contact of annealed particles [38], Further improving the stability of Ag_3PO_4-400 catalyst.

The surface composition and chemical status of the pristine Ag_3PO_4 and Ag_3PO_4-400 were evaluated by the XPS measurements in Fig. 2. The peak identification spectra of the two samples were similar and no obvious impurities can be detected (Figs. 2a and b). Figs. 2c and e show the binding energies for Ag 3d of the pristine Ag_3PO_4 and the annealed samples Ag_3PO_4-400. The two strong peaks with binding energy of 374.2 and 368.2 eV are attributed to $Ag_3d_{3/2}$ and $Ag_3d_{5/2}$, respectively. Figs. 2d and f show the O 1s peaks of pristine Ag_3PO_4 and Ag_3PO_4-400. By using Lorentziane Gaussian fitting, the O 1s peaks of the two samples were divided into two different peaks at 530.9 and 533.4 eV, respectively. The O 1s peak at 530.2 eV was usually attributed to the O^{2-} ions in Ag_3PO_4-400, while the other peak at 533.4 eV was related to the loosely bounded of OH or H_2O on the surface of Ag_3PO_4-400 [39,40]. Two kinds of oxygen concentration in the two samples were determined. The results showed that the bound oxygen content in the original Ag_3PO_4 and Ag_3PO_4-400 were 10.5% and 21.7%, respectively. OH or H_2O rich in the surface of Ag_3PO_4-400 may also play the same role as that rich in the surface of TiO_2, such as trapping photogenerated holes to promote carrier separation, generating more active radicals to improve photocatalytic activity.

The PL emission spectra can be carried out to disclose the efficiency of charge carrier trapping, transfer, and information about the recombination of free carriers [41], thus the lower PL intensity indicated the lower recombination rate of charge carriers [42]. The PL emission spectra of the as-prepared pristine Ag_3PO_4 and Ag_3PO_4-400 with the excitation wavelength of 325 nm at room temperature were compared and illustrated in Fig. S3. It can be found that these two samples exhibited the similar emission peaks in the visible-light range and a wide range of fluorescence emission of 400–540 nm, which was generally considered to be the reorganization of the valence band holes of the excitation conduction band electrons and semiconductors [43]. Obviously, the emission spectra of the Ag_3PO_4-400 decreased compared with that of the pristine Ag_3PO_4, indicating the energy-wasteful recombination process of electron–hole pairs can be inhibited effectively. These results showed that thermal annealing contributed to the effective separation of electron–hole pair, which may be one of the reasons for

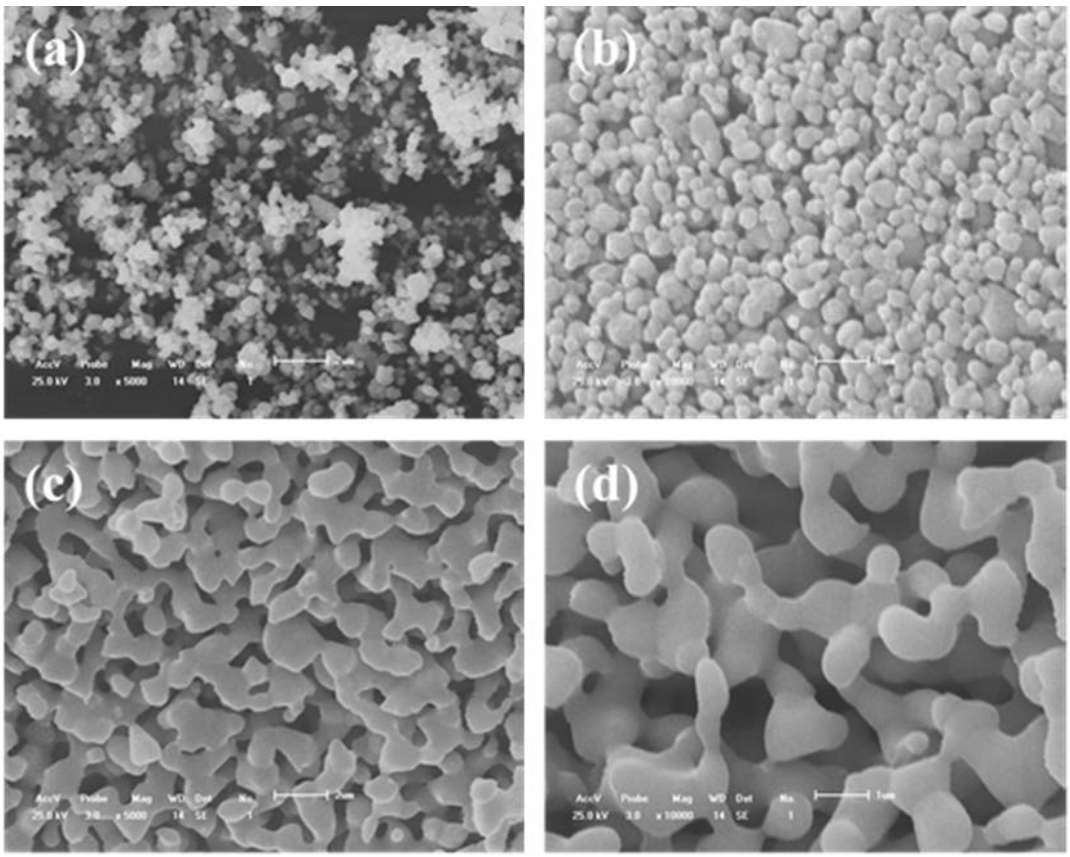

Fig. 1. SEM images of the Ag_3PO_4 and the pristine Ag_3PO_4-400 nano-powders at different magnifications: (a) Ag_3PO_4 × 5,000, (b) Ag_3PO_4 × 10,000, (c) Ag_3PO_4-400 × 5,000, and (d) Ag_3PO_4-400 × 10,000.

the enhancement of photocatalytic activity in Ag_3PO_4-400 samples under visible light irradiation.

To highlight the superior photocatalytic performance of the Ag_3PO_4-400 sample, the photocatalytic activities of the pristine Ag_3PO_4 and some reported Ag_3PO_4-based composite photocatalysts such as Ag_3PO_4/g-C_3N_4, Ag_3PO_4/WO_3, and Ag_3PO_4/ZnO were also tested under the same conditions. As illustrated in Fig. 3, the photocatalytic rate of β-naphthol degradation by the Ag_3PO_4-400 catalyst was higher than that of other catalysts, which was twice as high as that of the pristine Ag_3PO_4 catalyst. Moreover, almost no β-naphthol degradation occurred in the dark or in the absence of any photocatalyst, indicating light excitation and semiconductor photocatalyst were the essential factors for β-naphthol degradation.

3.2. Photocatalytic degradation

3.2.1. Effect of catalyst dosage

Ag_3PO_4-400 dosage in photocatalytic processes was an important factor that can strongly influence the degradation of β-naphthol. The dosage of 0.05, 0.10, 0.20, and 0.30 g of Ag_3PO_4-400 was used for examining the influence of catalyst dosage on β-naphthol removal and the results are shown in Fig. 4a. It can be observed that as the dosage of Ag_3PO_4-400 nanoparticles increased from 0.05 to 0.20 g, the efficiency increased from 63.4% to 99.8% within 6 min, while the amount of Ag_3PO_4-400 exceeded 0.20 g, the degradation ratio of β-naphthol slightly declined. The results show that with the increase of the amount of catalyst, the increase of reaction efficiency is mainly due to the increase of the number of active sites on Ag_3PO_4-400, which promoted the generation of active molecules. Above the optimum concentration of 0.20 g, the high concentration of Ag_3PO_4-400 would result in more light scattering and less ultraviolet light penetration. Moreover, particle agglomeration that occurred under high photocatalytic loading also can cause the deactivation of activated molecules and led to lower photodegradation efficiency.

3.2.2. Effect of initial concentration of β-naphthol

Photocatalytic degradation of β-naphthol was carried out using the catalyst Ag_3PO_4-400 with varying initial concentrations (10–50 mg/L) and the results were presented in Fig. 4b. It can be seen that as the concentration of β-naphthol increased, the photocatalytic efficiency decreased. When the initial β-naphthol concentration was 10 and 20 mg/L, the photocatalytic degradation efficiency was much higher than that of 30 and 50 mg/L. After 4 min reaction, the degradation rate of β-naphthol was decreased from 99.8% to 41.1% along with the increasing initial concentration of β-naphthol from 10 to 50 mg/L. As the concentration of β-naphthol increased, the removal rate of β-naphthol decreased remarkably.

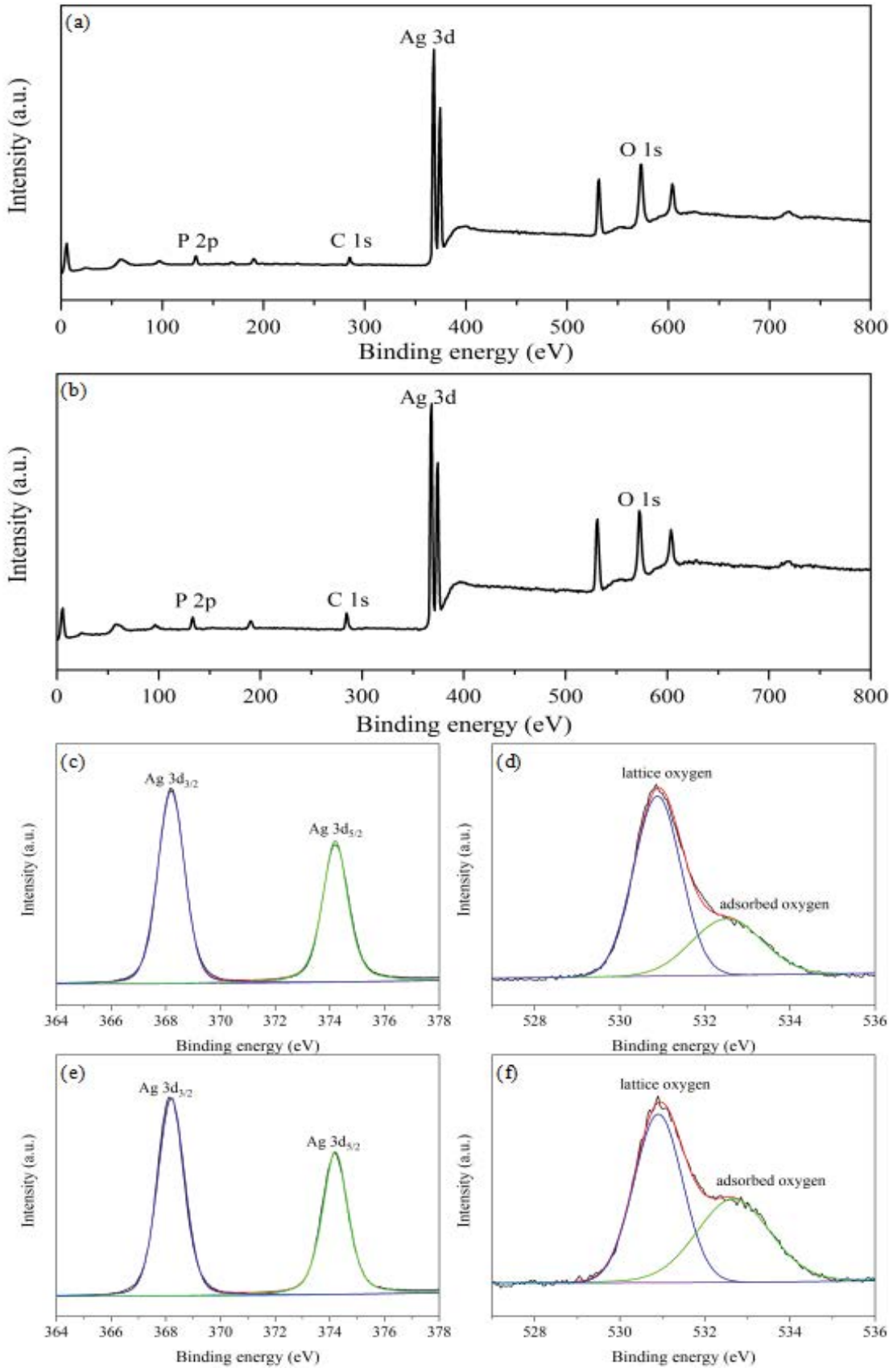

Fig. 2. (a) XPS spectra of pristine Ag_3PO_4, (b) XPS spectra of Ag_3PO_4-400, (c) Ag 3d of pristine Ag_3PO_4, (d) O 1s of pristine Ag_3PO_4, (e) Ag 3d of Ag_3PO_4-400, and (f) O 1s of Ag_3PO_4-400.

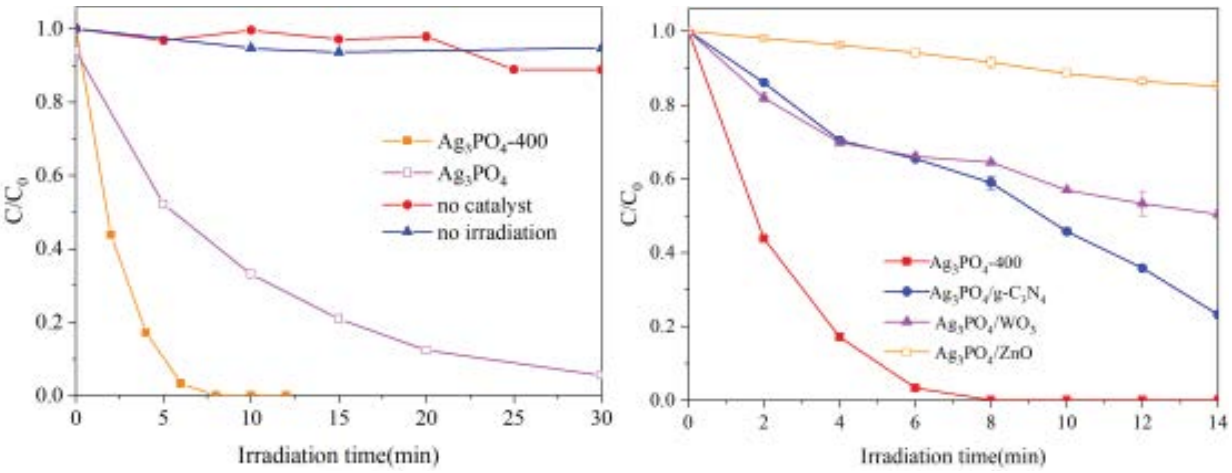

Fig. 3. Comparison photocatalytic activity for β-naphthol degradation over Ag_3PO_4-400 and pristine Ag_3PO_4 and some reported Ag_3PO_4-based composite photocatalysts (catalyst dosage = 0.1 g, C_0 = 20 mg/L, and pH = 6.8 ± 0.1).

It was due to the fact that at higher concentration, amount of β-naphthol and the intermediate products adsorbed on the photocatalyst surface might result in reduced number of active sites on the surface of catalyst, thus the generation of active species was reduced and hence inhibited its photocatalytic efficiency [44].

3.2.3. Effect of solution pH

One of the parameters influencing photocatalytic degradation was the pH of the solution, which can affect the adsorption capacity of the adsorbent in aqueous medium by altering the surface properties of adsorbent and shifting the potential of some redox reactions and also influencing the surface charge, size of the catalysts. In order to examine the effect of pH, the photocatalytic experiments at different pH values were determined. As shown in Fig. 4c, the degradation efficiency of β-naphthol was higher in the pH range of 3.0–12.0. Under the acidic medium (pH < 7) the system became positively charged (presence of H^+ ions), while it was became negatively charged in basic medium (pH > 7) due to OH^- ions. Ag_3PO_4-400 in water with negative charge at pH 3.0–12.0 (Fig. 4d), while the pKa of β-naphthol was 9.51, thus almost in this pH range studied it was mainly found in its molecular form. Therefore, the effect of pH on β-naphthol removal could be considered minor since the electrostatic attraction cannot occur. The photocatalytic efficiency of β-naphthol in weak acid, neutral, and weak base conditions is slightly higher than that in strong acid and alkaline conditions, which may be due to the solubility and instability of Ag_3PO_4-400 photocatalyst in strong acid and alkaline conditions.

3.2.4. Effect of the addition of humic acid

Humic acid (HA) is a major fraction of organic matter in natural waters or treated wastewaters, originating from animal and plant material breakdown. The effect of HA concentration on the photocatalytic efficiency of Ag_3PO_4-400 is shown in Fig. 4e. Photocatalytic degradation of β-naphthol was slightly enhanced by humic acid at a concentration of 1 mg/L, which may be due to its photosensitization effect [45] and the generation of other reactive oxygen species such as $^{\bullet}O_2^-$, $^1O_2$ by HA photolysis [46]. On the other hand, as the concentration of humic acid further increased, the photocatalytic efficiency gradually decreased. It may be attributed to the competitive adsorption of HA on Ag_3PO_4-400 active sites and attenuation of incident light in suspension resulting in reduced activation of Ag_3PO_4-400 [47].

3.2.5. Effect of inorganic salts

It should be noted that in addition to the organic matters contained in the actual wastewater, various inorganic salts would affect the photocatalytic efficiency. Therefore, considering this factor, we have studied the effect of NaCl, Na_2HPO_4, Na_2SO_4, and $NaNO_3$ on the photocatalytic removal of β-naphthol by Ag_3PO_4-400. The degradation of β-naphthol in the presence of 10 mm inorganic salt is shown in Fig. 4f. It can be observed that no appreciable change in the activity of the Ag_3PO_4-400 catalyst occurred in the solutions containing Na_2SO_4 and $NaNO_3$. When the Na_3PO_4 was added, the activity of the Ag_3PO_4-400 catalyst was reduced to some degree. The possible reason was that the high concentration of the PO_4^{3-} can induce high concentration of OH^-, and the solubility products (Ksp) of Ag_3PO_4 and AgOH were 8.89×10^{-17} and 2.0×10^{-8}, respectively. Obviously, AgOH was formed under the investigated conditions, while it was unstable and easily decomposed into Ag_2O and Ag. Compared with Ag_3PO_4, Ag_2O had a weaker photooxidation capability, resulting in a lower photocatalytic efficiency. We found that, the photocatalytic performance was significantly inhibited when NaCl was presenctin the system. This may be attributed to the formation of AgCl thick film (Ksp (AgCl) = 1.77×10^{-10}) on the surface of Ag_3PO_4, which inhibited the irradiation onto the Ag_3PO_4-400, so the photodegradation rate of β-naphthol was decreased.

3.3. Degradation mechanism

The reactive species trapping experiments were performed to investigate the predominant reactive oxygen

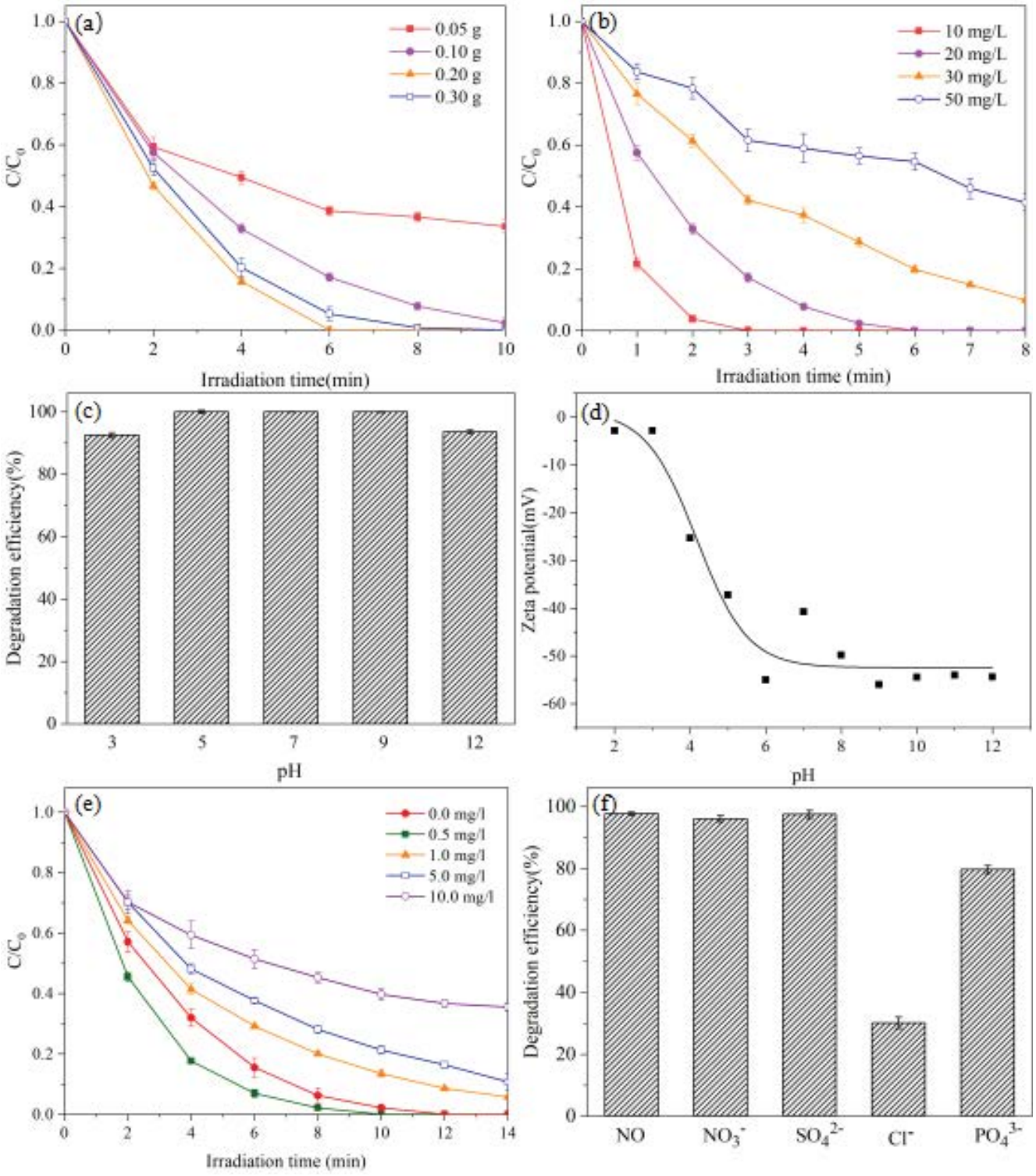

Fig. 4. Effect of (a) catalyst dosage on the photocatalytic degradation of β-naphthol, (b) initial β-naphthol concentrations, (c) pH, (d) zeta-potential of Ag_3PO_4-400, (e) addition of humic acid, and (f) inorganic salts.

species during the photocatalytic process by adding Ag_3PO_4-400 photocatalysts. In the experiments, isopropyl alcohol (IPA), benzoquinone (BQ), and ammoniumoxalate (AO) were separately introduced into the photocatalytic process and acted as the scavengers of hydroxyl radical ($^{\bullet}OH$), superoxide radicals ($^{\bullet}O_2^-$), and photoinduced holes (h^+). The concentration of all scavengers used was 1 mmol/L in the reaction and the result is shown in Fig. S4. It can be found that the addition of IPA to the β-naphthol solution had no apparent effect on photocatalytic activity. However, the

degradation efficiency decreased to 72.3% and 6.7% when BQ and AO were added into the reaction solution, respectively, indicating that h^+ and $^{\bullet}O_2^-$ indeed played an important role in the degradation of β-naphthol by Ag_3PO_4-400.

In order to more explicitly understand the degradation process of β-naphthol, GC-MS analysis was performed to identify the intermediate products of β-naphthol. The degradation pathway of β-naphthol and the molecular structure of intermediate products are shown in Fig. 5. It suggested that the photocatalytic degradation of β-naphthol using Ag_3PO_4-400 as photocatalyst was mainly occurred via h^+ and $^{\bullet}O_2^-$ attack. Due to the strong oxidation ability of the reactive groups, the benzene rings would be continuously destroyed, and the absence of hydroxylated intermediates indicated a relatively minor contribution of $^{\bullet}OH$ radicals to the degradation of β-naphthol. Based on the results above, the photocatalytic mechanism can be described as follows:

- Under simulated sunlight irradiation, the electron–hole pairs were separated by photons absorption of Ag_3PO_4-400. The electrons (e^-) in the valence band (VB) of Ag_3PO_4-400 can be excited to its conduction band (CB), leading to the generation of holes in the VB of Ag_3PO_4-400 simultaneously.

$$Ag_3PO_4\text{-}400 + hv \rightarrow e_{cb}^- + h_{vb}^+ \quad (1)$$

- $^{\bullet}O_2^-$ was produced by the reduction of oxygen molecules adsorbed on the catalyst surface by photogenerated electrons.

$$e_{cb}^- + (O_2)_{ads} \rightarrow {}^{\bullet}O^{2-} \quad (2)$$

- β-naphthol was directly degraded by the active species.

$$^{\bullet}O^{2-} + \beta\text{-naphthol} \rightarrow \text{Products} \quad (3)$$

$$^{\bullet}O^{2-} + \beta\text{-naphthol} \rightarrow \text{Products} \quad (4)$$

It has been confirmed that the intermediate products of naphthol degradation based on radicals can be further oxidized to stable small molecular aliphatic acids, such as maleic acid, malonic acid, oxalic acid, acrylic acid, formic acid, and acetic acid. Finally, these aliphatic organics can be adsorbed on the surface of the material and degraded into H_2O and CO_2 to realize the complete mineralization of naphthol [48].

3.4. Photocatalyst stability and regeneration

The photocatalyst stability was investigated by performing repeated photocatalytic tests using pristine Ag_3PO_4 and Ag_3PO_4-400. After each cycle, the catalysts were washed twice by distilled water and ethyl alcohol and then dried before using for the subsequent cycle. As shown in Fig. 6, even after five cycles, the Ag_3PO_4-400 also shows high photocatalytic activity, however, the photocatalytic degradation efficiency of Ag_3PO_4 decreased obviously that was only 40% of β-naphthol degradation occurred after four cycles.

During the consecutive cycles, electrons can be adopted by the Ag^+ released from the crystal lattice of Ag_3PO_4, thus leading to the deposition of Ag^0 on the surface, which could significantly reduce its photocatalytic activity [49]. A facile wet chemical–oxidation method was utilized to regenerate Ag_3PO_4-400, which was previously reported

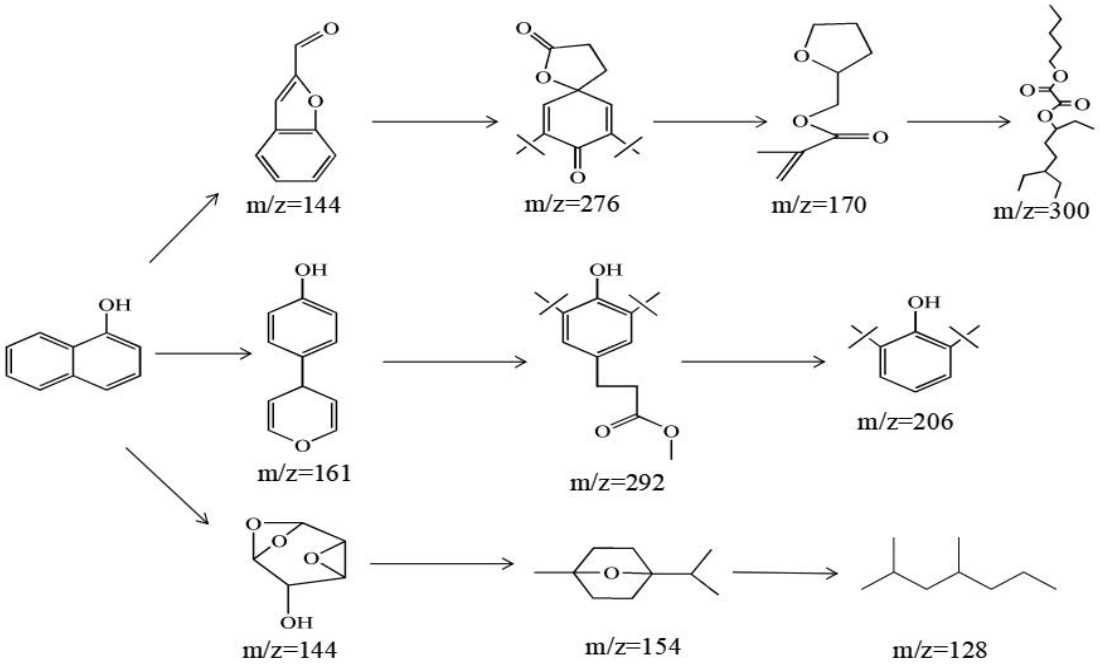

Fig. 5. Degradation pathway proposed on the basis of GC/MS analysis during photodegradation of β-naphthol.

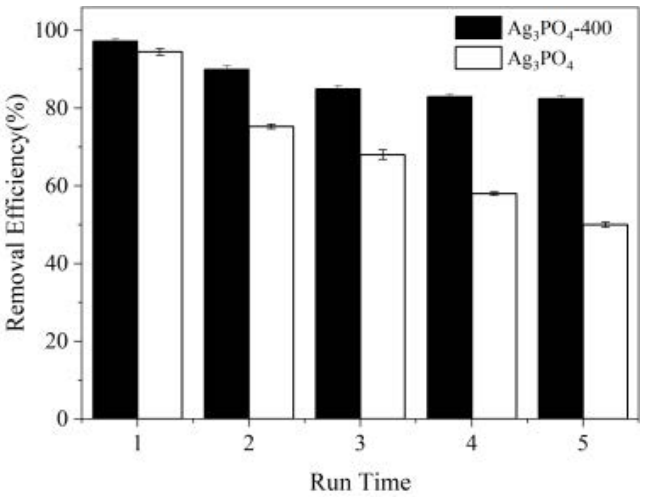

Fig. 6. Recycled experiments towards β-naphthol degradation over Ag_3PO_4-400 and pristine Ag_3PO_4 photocatalysts (catalyst dosage = 0.1 g, C_0 = 20 mg/L, and pH = 6.8 ± 0.1).

by Wang et al. [50]. During the regeneration process, H_2O_2 can oxidize Ag to Ag^+, while the acid environment of aqueous solution also can dissolve Ag_3PO_4-400, and the rapid decomposition of H_2O_2 occurred, thus weaker alkaline sodium ammonium hydrogen phosphate tetrahydrate was chosen as PO_4^{3-} source. As shown in Fig. S5, the photocatalytic activity of the regenerated Ag_3PO_4-400 was not as good as that of the fresh Ag_3PO_4-400 nanoparticles. However, the photocatalytic activity of the regenerated Ag_3PO_4-400 was retained at >92.6% of its original activity, indicating a successful rejuvenation of Ag_3PO_4-400.

4. Conclusion

In summary, a novel Ag_3PO_4-400 photocatalyst was successfully synthesized using a simple and efficient thermal annealing technique which exhibited the enhanced photocatalytic degradation of β-naphthol under visible light irradiation. The photocatalyst Ag_3PO_4-400 was found to be more efficient as compared with other reported Ag_3PO_4-based composite photocatalysts. The band gap of Ag_3PO_4-400 catalyst was wider than Ag_3PO_4, and the quantum efficiency of Ag_3PO_4-400 is higher than that of Ag_3PO_4. The photocatalytic activity was inhibited by the high concentration of β-naphthol. The addition of NO_3^- and SO_4^{2-} into the reaction solution had practically little influence on the degradation of β-naphthol, however, the degradation rate was significantly reduced by the addition of Cl^- and PO_4^{3-}. The presence of humic acid at small concentrations can lead to a higher degradation efficiencies, but as the concentration of humic acid increased, the inhibitory effect gradually increased. The main active species that responsible for the degradation of β-naphthol were recognized as $^{\bullet}O_2^-$ and h^+ through trapping experiments. Moreover, after thermal annealing, the photocatalyst Ag_3PO_4-400 showed higher stability during β-naphthol removal than the pristine Ag_3PO_4. The experimental results showed that the regenerated method almost completely restored catalyst activity, indicating a promising prospect of practical application of Ag_3PO_4 in the environmental remediation.

Acknowledgments

The authors acknowledge financial support from the National Key Research and Development Program of China (No. 2019YFC1805300), the National Natural Science Foundation of China (NSFC) (No. 41972257), and the Fundamental Research Funds for the Central Universities (No. 2652019281). In addition, we are grateful to the editor and two anonymous reviewers for their suggestions, which are essential for us to improve the content of the article.

References

[1] C.E. Cerniglia, C.C. Somerville, Reductive Metabolism of Nitroaromatic and Nitropolycyclic Aromatic Hydrocarbons, Springer US, 1995. Available at: http://link.springer.com/10.1007/978-1-4757-9447-2_7.
[2] W. Sirisaksoontorn, S. Thachepan, A. Songsasen, Photodegradation of phenanthrene by N-doped TiO_2 photocatalyst, Environ. Lett., 44 (2009) 841–846.
[3] C. Croera, D. Ferrario, L. Gribaldo, *In vitro* toxicity of naphthalene, 1-naphthol, 2-naphthol and 1,4-naphthoquinone on human CFU-GM from female and male cord blood donors, Toxicol. in Vitro, 22 (2008) 1555–1561.
[4] S. Zang, B. Lian, Synergistic degradation of 2-naphthol by *Fusarium proliferatum* and *Bacillus subtilis* in wastewater, J. Hazard. Mater., 166 (2009) 33–38.
[5] J. Huang, B. Yuan, X. Wu, S. Deng, A comparative adsorption study of β-naphthol on four polymeric adsorbents from aqueous solutions, J. Colloid Interface Sci., 380 (2012) 166–172.
[6] S. Qourzal, N. Barka, M. Tamimi, A. Assabbane, Y. Ait-Ichou, Photodegradation of 2-naphthol in water by artificial light illumination using TiO_2 photocatalyst: identification of intermediates and the reaction pathway, Appl. Catal., A, 334 (2008) 386–393.
[7] K.H. Wang, Y.H. Hsieh, L.J. Chen, The heterogeneous photocatalytic degradation, intermediates and mineralization for the aqueous solution of cresols and nitrophenols, J. Hazard. Mater., 59 (1998) 251–260.
[8] D. Bahnemann, Photocatalytic water treatment: solar energy applications, Sol. Energy, 77 (2004) 445–459.
[9] Y. Hu, C. Yuan, Low-temperature preparation of photocatalytic TiO_2 thin films from anatase sols, J. Cryst. Growth, 274 (2005) 563–568.
[10] G. Sivalingam, G. Madras, Photocatalytic degradation of poly(bisphenol-A-carbonate) in solution over combustion-synthesized TiO_2: mechanism and kinetics, Appl. Catal., A, 269 (2004) 81–90.
[11] H. Tang, Y. Fu, S. Chang, S. Xie, G. Tang, Construction of Ag_3PO_4/Ag_2MoO_4 Z-scheme heterogeneous photocatalyst for the remediation of organic pollutants, Chin. J. Catal., 38 (2016) 337–347.
[12] G.F. Huang, Z.L. Ma, W.Q. Huang, Y. Tian, C. Jiao, Z.M. Yang, Z. Wan, A. Pan, Ag_3PO_4 semiconductor photocatalyst: possibilities and challenges, J. Nanomater., 2013 (2013) 1–8, doi: 10.1155/2013/371356.
[13] Z. Frontistis, M. Antonopoulou, A. Petala, D. Venieri, I. Konstantinou, D.I. Kondarides, D. Mantzavinos, Photodegradation of ethyl paraben using simulated solar radiation and Ag_3PO_4 photocatalyst, J. Hazard. Mater., 323 (2017) 478–488.
[14] W. Yao, B. Zhang, C. Huang, C. Ma, X. Song, Q. Xu, Synthesis and characterization of high efficiency and stable Ag_3PO_4/TiO_2 visible light photocatalyst for the degradation of methylene blue and rhodamine B solutions, J. Mater. Chem., 22 (2012) 4050–4055.
[15] J. Wang, F. Teng, M. Chen, J. Xu, Y. Song, X. Zhou, Facile synthesis of novel Ag_3PO_4 tetrapods and the {110} facets-dominated photocatalytic activity, CrystEngComm, 15 (2012) 39–42.

[16] A. Wu, C. Tian, C. Wei, H. Yu, Q. Zhang, Q. Yang, H. Fu, Morphology-controlled synthesis of Ag_3PO_4 nano/microcrystals and their antibacterial properties, Mater. Res. Bull., 48 (2013) 3043–3048.
[17] J. Wan, E. Liu, J. Fan, X. Hu, L. Sun, C. Tang, Y. Yin, H. Li, Y. Hu, *In-situ* synthesis of plasmonic Ag/Ag_3PO_4 tetrahedron with exposed {111} facets for high visible-light photocatalytic activity and stability, Ceram. Int., 41 (2015) 6933–6940.
[18] H. Yu, G. Cao, F. Chen, X. Wang, J. Yu, M. Lei, Enhanced photocatalytic performance of Ag_3PO_4 by simutaneous loading of Ag nanoparticles and Fe(III) cocatalyst, Appl. Catal., B, 160–161 (2014) 658–665.
[19] F.M. Zhao, L. Pan, S. Wang, Q. Deng, J.J. Zou, L. Wang, X. Zhang, Ag_3PO_4/TiO_2 composite for efficient photodegradation of organic pollutants under visible light, Appl. Surf. Sci., 317 (2014) 833–838.
[20] D. Wang, L. Li, Q. Luo, J. An, X. Li, R. Yin, M. Zhao, Enhanced visible-light photocatalytic performances of Ag_3PO_4 surface-modified with small amounts of TiO_2 and Ag, Appl. Surf. Sci., 321 (2014) 439–446.
[21] Z. Xiu, H. Bo, Y. Wu, X. Hao, Graphite-like C_3N_4 modified Ag_3PO_4 nanoparticles with highly enhanced photocatalytic activities under visible light irradiation, Appl. Surf. Sci., 289 (2014) 394–399.
[22] C. Li, Q. Long, C. Yin, Synthesis and characterization of high photocatalytic activity and stable Ag_3PO_4/TiO_2 fibers for photocatalytic degradation of black liquor, Appl. Surf. Sci., 319 (2014) 60–67.
[23] Z. Song, X. Dong, N. Wang, L. Zhu, Z. Luo, J. Fang, C. Xiong, Efficient photocatalytic defluorination of perfluorooctanoic acid over BiOCl nanosheets via a hole direct oxidation mechanism, Chem. Eng. J., 317 (2017) 925–934.
[24] X. Gao, W. Peng, G. Tang, Q. Guo, Y. Luo, Highly efficient and visible-light-driven BiOCl for photocatalytic degradation of carbamazepine, J. Alloys Compd., 757 (2018) 455–465.
[25] W.W. Liu, R.F. Peng, Recent advances of bismuth oxychloride photocatalytic material: property, preparation and performance enhancement, J. Electron. Sci. Technol., (2020) 119–137, doi: 10.1016/j.jnlest.2020.100020.
[26] W. Liu, Z. Dai, L. Yi, A. Zhu, D. Zhong, J. Wang, J. Pan, Intimate contacted two-dimensional/zero-dimensional composite of bismuth titanate nanosheets supported ultrafine bismuth oxychloride nanoparticles for enhanced antibiotic residue degradation, J. Colloid Interface Sci., 529 (2018) 23–33.
[27] J. Xie, Y. Yang, H. He, D. Cheng, M. Mao, Q. Jiang, L. Song, J. Xiong, Facile synthesis of hierarchical Ag_3PO_4/TiO_2 nanofiber heterostructures with highly enhanced visible light photocatalytic properties, Appl. Surf. Sci., 355 (2015) 921–929.
[28] K. Zhu, N.R. Neale, A.F. Halverson, Y.K. Jin, A.J. Frank, Effects of annealing temperature on the charge-collection and light-harvesting properties of TiO_2 nanotube-based dye-sensitized solar cells, J. Phys. Chem. C, 114 (2010) 13433–13441.
[29] J. Lin, M. Guo, C.T. Yip, W. Lu, G. Zhang, X. Liu, L. Zhou, X. Chen, H. Huang, High temperature crystallization of free-standing anatase TiO_2 nanotube membranes for high efficiency dye-sensitized solar cells, Adv. Funct. Mater., 23 (2013) 5952–5960.
[30] J. Yu, H. Yu, B. Cheng, X. Zhao, J.C.Y. And, W.K. Ho, The effect of calcination temperature on the surface microstructure and photocatalytic activity of TiO_2 thin films prepared by liquid phase deposition, J. Phys. Chem. B, 107 (2003) 13871–13879.
[31] C.Q. Xu, K. Li, W.D. Zhang, Enhancing visible light photocatalytic activity of nitrogen-deficient g-C_3N_4 via thermal polymerization of acetic acid-treated melamine, J. Colloid Interface Sci., 495 (2017) 27–36.
[32] X. Xing, M. Zhang, L. Hou, L. Xiao, Q. Li, J. Yang, Z-scheme BCN-TiO_2 nanocomposites with oxygen vacancy for high efficiency visible light driven hydrogen production, Int. J. Hydrogen Energy, 42 (2017) 28434–28444.
[33] X. Guo, N. Chen, C. Feng, Y. Yang, B. Zhang, G. Wang, Z. Zhang, Performance of magnetically recoverable core–shell Fe_3O_4@ Ag_3PO_4/AgCl for photocatalytic removal of methylene blue under simulated solar light, Catal. Commun., 38 (2013) 26–30.
[34] L. Ghalamchi, S. Aber, V. Vatanpour, M. Kian, A novel antibacterial mixed matrixed PES membrane fabricated from embedding aminated Ag_3PO_4/g-C_3N_4 nanocomposite for use in the membrane bioreactor, J. Ind. Eng. Chem., 70 (2019) 412–426.
[35] L. Wang, J. Liu, Y. Wang, X. Zhang, D. Duan, C. Fan, Y. Wang, Insight into the enhanced photocatalytic performance of Ag_3PO_4 modified metastable hexagonal WO_3, Colloids Surf., A, 541 (2018) 145–153.
[36] C. Dong, K.L. Wu, M.R. Li, L. Liu, X.W. Wei, Synthesis of Ag_3PO_4–ZnO nanorod composites with high visible-light photocatalytic activity, Catal. Commun., 46 (2014) 32–35.
[37] J.W. Park, S.G. Baek, Thermal behavior of direct-printed lines of silver nanoparticles, Scr. Mater., 55 (2006) 1139–1142.
[38] T. Yan, W. Guan, J. Tian, P. Wang, W. Li, J. You, B. Huang, Improving the photocatalytic performance of silver phosphate by thermal annealing: influence of acetate species, J. Alloys Compd., 680 (2016) 436–445.
[39] H. Wang, Y. Bai, J. Yang, X. Lang, J. Li, L. Guo, A facile way to rejuvenate Ag_3PO_4 as a recyclable highly efficient photocatalyst, Chem. Eur. J., 18 (2012) 5524–5529.
[40] J.C.C. Fan, J.B. Goodenough, X-ray photoemission spectroscopy studies of Sn-doped indium-oxide films, J. Appl. Phys., 48 (1977) 3524–3531.
[41] X.Z.L. And, F.B. Li, Study of Au/Au^{3+}-TiO_2 photocatalysts toward visible photooxidation for water and wastewater treatment, Environ. Sci. Technol., 35 (2001) 2381–2387.
[42] L. Jing, Y. Qu, B. Wang, S. Li, B. Jiang, L. Yang, W. Fu, H. Fu, J. Sun, Review of photoluminescence performance of nano-sized semiconductor materials and its relationships with photocatalytic activity, Sol. Energy Mater. Sol. Cells, 90 (2006) 1773–1787.
[43] Y. Wang, W. Kang, X. Wang, Preparation of $Ag_3PO_4/Ni_3(PO_4)_2$ hetero-composites by cation exchange reaction and its enhancing photocatalytic performance, J. Colloid Interface Sci., 466 (2015) 178–185.
[44] U.G. Akpan, B.H. Hameed, Parameters affecting the photocatalytic degradation of dyes using TiO_2-based photocatalysts: a review, J. Hazard. Mater., 170 (2009) 520–529.
[45] K. Vinodgopal, P.V. Kamat, Photochemistry on surfaces: photodegradation of 1,3-diphenylisobenzofuran over metal oxide particles, J. Phys. Chem., 96 (1992) 5053–5059.
[46] H. Xu, W.J. Cooper, J. Jung, W. Song, Photosensitized degradation of amoxicillin in natural organic matter isolate solutions, Water Res., 45 (2011) 632–638.
[47] V. Repousi, A. Petala, Z. Frontistis, M. Antonopoulou, I. Konstantinou, D.I. Kondarides, D. Mantzavinos, Photocatalytic degradation of bisphenol A over Rh/TiO_2 suspensions in different water matrices, Catal. Today, 284 (2016) 59–66.
[48] G. Jayamani, M. Shanthi, An efficient nanocomposite CdS-$ZnWO_4$ for the degradation of Naphthol Green B dye under UV-A light illumination, Nanostruct. Nanoobjects, 22 (2020) 1–14, doi: 10.1016/j.nanoso.2020.100452.
[49] C. Zhou, Y. Zhao, J. Cao, H. Lin, S. Chen, Partial oxidation controlled activity regeneration of used Ag_3PO_4 photocatalyst via removing the *in situ* surface metallic silver, Appl. Surf. Sci., 351 (2015) 33–39.
[50] Y. Wang, J. Liu, Y. Wang, C. Fan, G. Ding, Regeneration of novel visible-light-driven Ag/Ag_3PO_4@C_3N_4 hybrid materials and their high photocatalytic stability, Mater. Sci. Semicond. Process., 25 (2014) 330–336.

Supplementary information

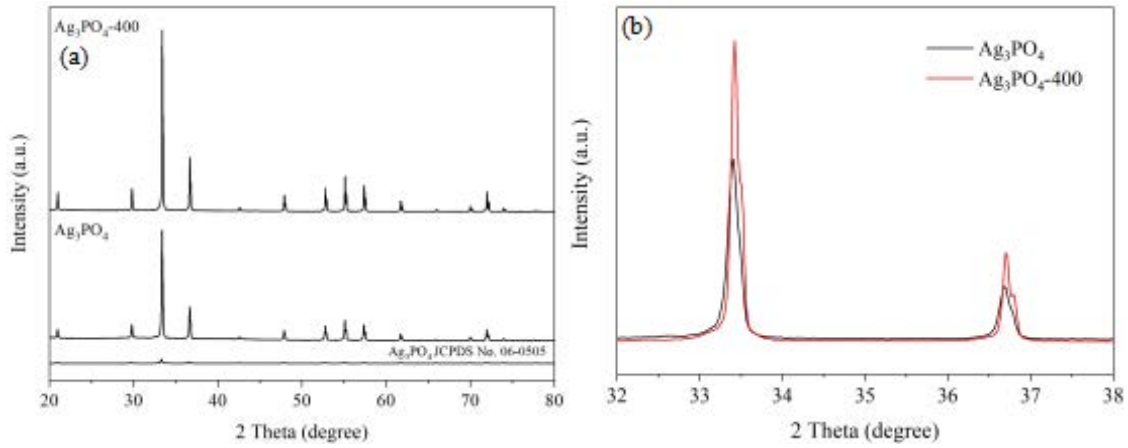

Fig. S1. (a) XRD pattern of the Ag_3PO_4-400 and the pristine Ag_3PO_4 photocatalysts, (b) partially enlarged XRD patterns of the Ag_3PO_4-400 and the pristine Ag_3PO_4 photocatalysts.

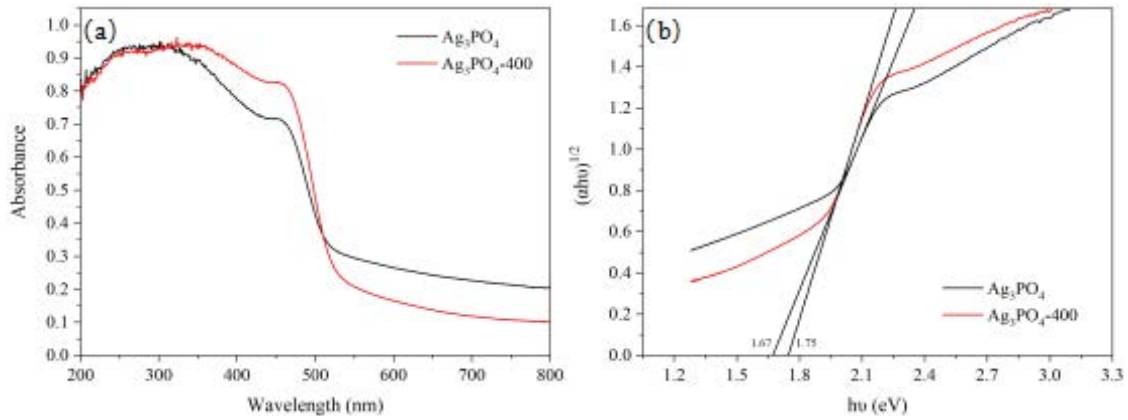

Fig. S2. (a) UV-vis diffuse reflectance spectra and (b) band energy of samples.

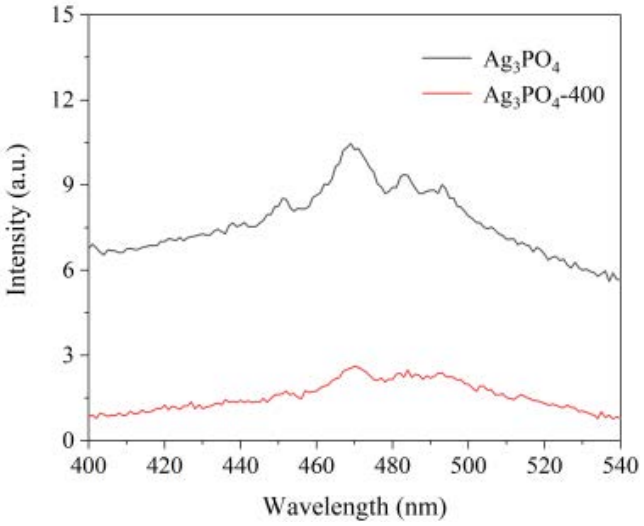

Fig. S3. PL spectra of pristine Ag_3PO_4 and Ag_3PO_4-400.

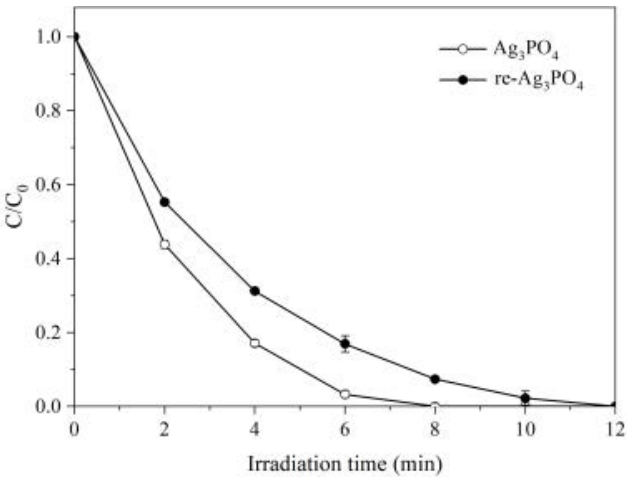

Fig. S5. Photocatalytic activities of the fresh Ag_3PO_4-400 and the rejuvenated Ag_3PO_4-400 (catalyst dosage = 0.1 g, C_0 = 20 mg/L, and pH = 6.8 ± 0.1).

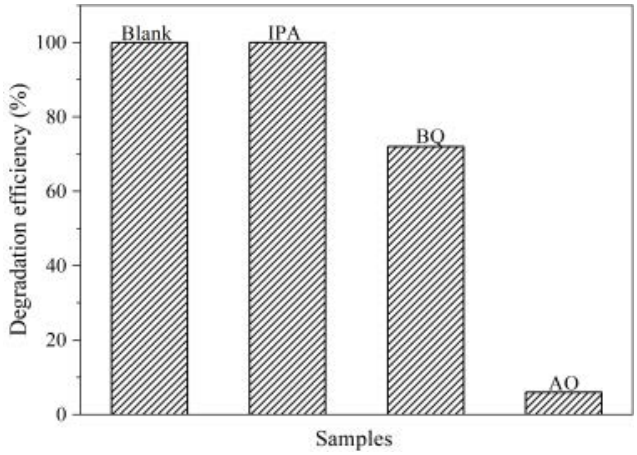

Fig. S4. Photodegradation of β-naphthol on Ag_3PO_4-400 in the presence of different scavengers (catalyst dosage = 0.1 g, C_0 = 20 mg/L, and pH = 6.8 ± 0.1).